






Article

Influence of BRDF Models and Solar Zenith Angles on Forest Above-Ground Biomass Derived from MODIS Multi-Angular Indices

Lei Cui ^{1,2}, Jiaying Zhang ^{2,*}, Yiqun Dai ², Rui Xie ³, Zhongzheng Zhu ⁴, Mei Sun ⁵, Xiaoning Zhang ⁶, Long He ², Hu Zhang ², Yadong Dong ⁷ and Kaiguang Zhao ⁸

- ¹ Navigation College, Jimei University, Xiamen 361001, China; cui@mail.bnu.edu.cn
 - ² Faculty of Geographical, Tianjin Normal University, Tianjin 300387, China; 2130080260@stu.tjnu.edu.cn (Y.D.); longhe@tjnu.edu.cn (L.H.); huzhang@tjnu.edu.cn (H.Z.)
 - ³ International Institute for Earth System Science, Nanjing University, Nanjing 210023, China; xierui@mail.bnu.edu.cn
 - ⁴ National Tibetan Plateau Data Center (TPDC), State Key Laboratory of Tibetan Plateau Earth System Science, Environment and Resources (TPESER), Institute of Tibetan Plateau Research, Chinese Academy of Sciences, Beijing 100101, China; zhuzz@itpcas.ac.cn
 - ⁵ Industrial Technology Research Institute, Xiamen University of Technology, Xiamen 361024, China; sunm@xmut.edu.cn
 - ⁶ School of Mechatronical Engineering, Beijing Institute of Technology, Beijing 100081, China; xnzhang@bit.edu.cn
 - ⁷ State Key Laboratory of Remote Sensing Science, Jointly Sponsored by Beijing Normal University and Aerospace Information Research Institute of Chinese Academy of Sciences, Beijing Normal University, Beijing 100875, China; dongyd@aircas.ac.cn
 - ⁸ School of Environment and Natural Resources, The Ohio State University, Wooster, OH 43210, USA; zhao.1423@osu.edu
- * Correspondence: 2130080285@stu.tjnu.edu.cn



Citation: Cui, L.; Zhang, J.; Dai, Y.; Xie, R.; Zhu, Z.; Sun, M.; Zhang, X.; He, L.; Zhang, H.; Dong, Y.; et al. Influence of BRDF Models and Solar Zenith Angles on Forest Above-Ground Biomass Derived from MODIS Multi-Angular Indices. *Forests* **2024**, *15*, 541. <https://doi.org/10.3390/f15030541>

Academic Editor: José Aranha

Received: 27 February 2024

Revised: 6 March 2024

Accepted: 12 March 2024

Published: 15 March 2024



Copyright: © 2024 by the authors. Licensee MDPI, Basel, Switzerland. This article is an open access article distributed under the terms and conditions of the Creative Commons Attribution (CC BY) license (<https://creativecommons.org/licenses/by/4.0/>).

Abstract: Multi-angular remote sensing observation contains crucial information on forest structure parameters. Here, our goal is to examine the ability of multi-angular indices, which are constructed by the typical-angular reflectances in red and NIR bands from MODIS observations, for the retrieval of forest biomass based on the field-measured above-ground biomass (AGB) data. Specifically, we employed the updated version of the MCD43A1 BRDF parameter product as an input for BRDF models to reconstruct the MODIS typical-angular reflectances. Furthermore, we evaluated the effects of different configurations of BRDF models and solar zenith angles (SZA) on forest AGB estimation using our developed multi-angular indices. The semivariogram analysis strategy combined with Landsat ground-surface reflectance data was employed to determine the MODIS pixel heterogeneity; the survey data from field sites of homogeneous pixels was used in our analysis and validation. The results show that our developed multi-angular indices based on a hot-revised BRDF model, under a SZA of 45°, when combined with forest cover information, can account for up to 72% of the variation forest AGB, with an RMSE = 45 Mg/ha. We also found that different kernels for the BRDF models influenced the weight parameters of the biomass inversion equation but did not significantly affect the estimated AGB. In conclusion, our method can enable the better usage of MODIS multi-angular observations for forest AGB estimation.

Keywords: MODIS; typical-angular reflectances; multi-angular indices; BRDF models; forest aboveground biomass

1. Introduction

Forest aboveground biomass (AGB) is closely related to the carbon sinks of forest ecosystems and is important for greenhouse gas inventories and terrestrial carbon accounting [1,2]. Accurate, large-scale, wall-to-wall maps of forest AGB can help address the above

issues [3]. Researchers widely used different types of remote sensing images for AGB estimation and presented valuable results in this way [4,5]. However, most of these methods are inadequate because they lack explicit information on canopy three-dimensional structures. Fortunately, multi-angular remote sensing technology, which has been proven to be sensitive to forest 3D structures [6–8], provides a promising solution for inverting high-quality and wall-to-wall forest AGB maps.

Multi-angular remote sensing involves capturing surface reflectance from various view angles, including angles beyond the nadir, while also accounting for the sun's position. This observation technology enables the measurement of the anisotropic reflectance of the land surface. Anisotropic surface reflectances, which can be indicated by the bidirectional reflectance distribution function (BRDF), describe the uneven distribution of the forest canopy on the surface [9,10]. In other words, BRDF information provided by multi-angular satellite observation was considered to contain the 3D structure feature information of ground targets in theory [11,12]. Therefore, BRDF information has the potential to inversion vegetation structure parameters.

Recently, multi-angular remote sensing provided BRDF information that has been employed on forest AGB estimation. Some estimation methods employed a multivariable regression strategy to develop models based on MODIS data (red and near-infrared BRFs) to retrieve AGB [13]. Multi-angular observations from Multi-angle Imaging Spectro Radiometer (MISR) were also employed as input variables to develop regression relationships with AGB, such as MISR red band bidirectional reflectances from different views [14,15]; a \log_e relationship was also found between MISR multi-angular surface reflectance data and AGB estimates [16]. Some spectral vegetation indices developed from multi-angular reflectances were used to estimate forest AGB, mainly through regression or the look-up table strategy [17,18]. A recent study found that forest biomass structure information was embedded in the typical directional multi-angular reflectance observed from the red and NIR spectral bands [19], highlighting a promising new source for forest AGB inversion.

Prior research has showcased the efficacy of multi-angular measurements in estimating forest AGB, especially concerning typical-angular reflectances. However, acquiring specific multi-angular reflectances via satellite can be challenging, such as reflectances at the hotspot and darkspot directions. Consequently, the retrieval relies on the BRDF models. Hence, the accuracy of forest AGB estimation may be influenced by the selection of BRDF models, as different models exhibit varying abilities to characterize specific BRDF features, particularly reflectances at high solar zenith angles (SZAs) [20,21].

The BRDF model is a semi-empirical linear model that typically comprises geometric optics (GO) and volumetric scattering kernels. Various forms of these kernels have been developed for different scenarios and objectives [22–24]. The RossThick (RT) kernel, based on Radiative Transfer Theory, was the first volumetric kernel to be developed [22]. To address scenarios with a small leaf area index (LAI), the RossThin (RTIN) kernel was developed [23]. In terms of the GO kernel, the LiSparse (LS) and LiDense (LD) kernels were deduced based on the GO theory developed by Li and Strahler [23,25]. These two kernels describe the sparse and dense canopy structures, respectively. The LiSparseR (LSR) and LiDenseR (LDR) GO kernels that satisfy the reciprocity principle are defined afterward by considering that the reflection component varies with the SZA [24]. Aiming to enhance the performance of the LSR kernel at large SZAs, the LiTransitR (LTR) kernel was proposed by combining LSR and LDR kernels [25]. To enhance the kernel-driven BRDF model's accuracy in estimating hotspot reflectance, several approaches have been explored. For example, researchers developed a RossThickChen (RTC) kernel, a volume-scattering kernel revised specifically for hotspot correction [26], which has been successfully used to improve the inversion accuracy of vegetation structure parameters [12,19].

Despite the advancement of various BRDF models, all these models are designed for different scenes and purposes. Therefore, the selection of the most suitable BRDF model to reconstruct multi-angular reflectances for vegetation structure parameter inversion, such as forest AGB, needs further evaluation. This study aims to assess the influence

of various configurations of BRDF models in estimating forest AGB using multi-angular indices. Specifically, we developed three multi-angular indices, which were formulated by the typical-angular reflectances in red and NIR spectral bands, combined with forest cover information to build the forest AGB estimation equation. The typical-angular reflectances were constructed by using the updated MCD43A1 MODIS parameter product (version 6.1), which served as the input for the BRDF model. We selected seven widely used BRDF models in our research; they are constructed by the volume-scattering kernels RT, RTIN, and RTC, and GO kernels LSR, LDR, and LTR. A semivariance function was employed to determine the homogeneous MODIS pixel, and the corresponding survey data of field-measured sites was used to validate. We further assess the potential influence on the MODIS–AGB relationship from factors such as forest cover density.

The novelties of this study are as follows: (i) the potential of multi-angular observations to estimate forest AGB was assessed using MODIS data; (ii) the new multi-angular indices were developed to estimate forest AGB; (iii) the robustness and generalization power of the multi-angular indices were assessed, especially from the selection of BRDF models and solar zenith angles; and (iv) the influence of pixel forest cover density and terrain on the performance of multi-angular indices were assessed.

2. Materials

2.1. Study Sites

We used field measurements that were distributed at five New England environmental forest stations, which are located on the eastern coast of three states in the United States. The forests include the Bartlett Experimental Forest, Hubbard Brook Experimental Forest, Howland Research Forest, Penobscot Experimental Forest, and Harvard Forest; the field measurement sites in these forests can be found in Figure 1. The terrain of these research sites includes flat areas, hills, and valleys with steep slopes. The climate in these sites has warm summers and cold winters. Most of the sites' mean annual precipitation is around 1000 mm. These sites have differences in soil composition; most of the sites are predominantly a sandy loam glacial till with moderate to good drainage. Forest species distributions in our study areas are primarily shaped by climate, which is also influenced by altitude. The dominant species include the northern white cedar (*Thuja occidentalis*), balsam fir (*Abies balsamea*), red spruce (*Picea rubens*), and eastern hemlock (*Tsuga canadensis*). Detailed information about these study sites can be found on NASA EARTHDATA's official website [27].

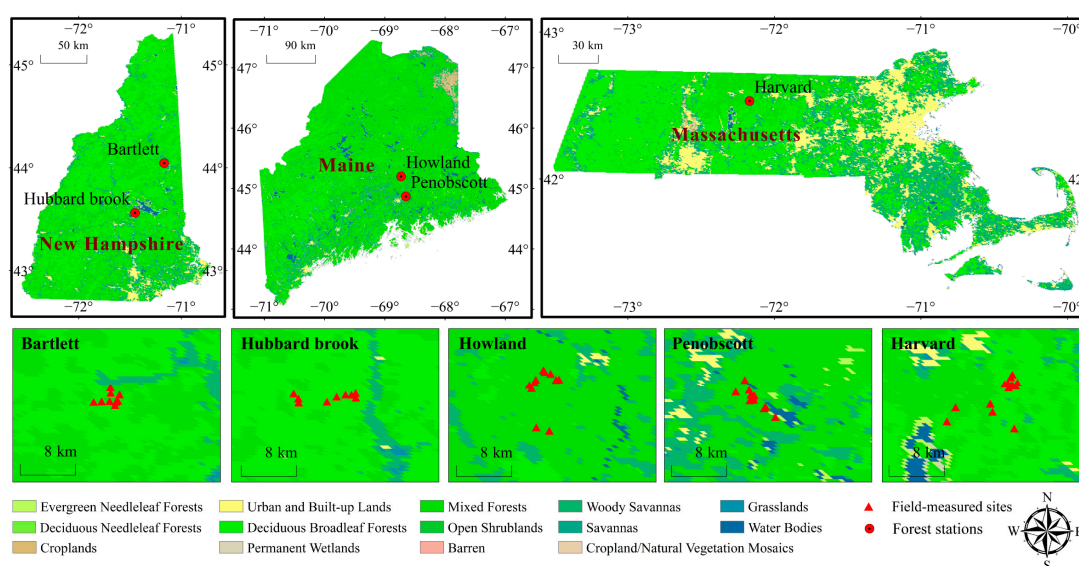


Figure 1. Locations of field-measured plots are at five New England experimental forest stations. Bartlett and Hubbard Brook Forests are in New Hampshire; Howland and Penobscot Forests are in Maine; Harvard Forest is in Massachusetts.

2.2. Field-Measured Biomass Data

We utilized field-measured biomass data as a benchmark to assess the efficacy of BRDF information in estimating forest AGB. The field-measured biomass data used in this study was sourced from the North American Carbon Program (NACP). All the biomass data from field measurements were gathered within a plot measuring 50 m by 200 m. In each plot, the tree with a diameter at breast height (DBH) of 10 cm or more (measured at 1.3 m) was recorded. Furthermore, tree species and living conditions for the recorded trees were recorded (Appendix A). We used forest biomass data calculated based on an allometric equation from Young et al. 1980: $\ln(\text{AGB}) = B_0 + B_1(\ln(\text{DBH}))$; B_0 and B_1 are provided by a weight table for tree species [28]. The basic information about the field-measured biomass data can be found in the NACP of NASA projects [27]; a total of 55 field-measured AGB datasets were used in this study.

2.3. MODIS BRDF Data

We utilized version 6.1 of the MODIS BRDF/Albedo Model Parameters Product (MCD43A1) for the red and NIR spectral bands as input to the BRDF model for calculating the typical-angular reflectances. The MCD43A1 dataset recorded the BRDF model weighting parameters, including weights for isotropic, volumetric, and geometric parameters. These weighting parameters describe the bidirectional reflectance properties of the land surface across various spectral bands, each with a spatial resolution of 500 m. We employed the version 6.1 dataset of the MCD43A1 product, which has been improved by various calibration changes [29]. We prefer to use high-quality data from the MCD43A1 product in this study. To address the absence of high-quality data resulting from cloud contamination at certain times, we implemented a strategy to fill in missing data by incorporating high-quality full inversion data ($QA = 0$) obtained from a month closely matching the timing of field measurements. This approach assumes that the forest's structure undergoes minimal changes within a one-month period, thereby limiting the potential impact of our strategy on the study results.

2.4. Landsat Surface Reflectance Data

Landsat surface reflectance data is a good option for delineating surface material differences [30,31], making it a common choice for pixel heterogeneity analysis [32,33]. Consistent with prior studies, we utilized Landsat surface reflectance data to assess the homogeneity of MODIS pixels. The following is the reason why we conducted pixel homogeneity analysis: we utilized field-measured forest biomass as the reference for AGB in the corresponding MODIS pixel. However, a potential concern arises regarding whether the ground-observed data accurately represents the true conditions of the MODIS pixel. It is generally assumed that for homogeneous pixels, ground observations can reasonably reflect the characteristics of the pixel at a larger scale. To validate the representativeness of the ground observation data for the actual conditions at the MODIS pixel scale, we utilized 30 m of Landsat surface reflectance data under clear sky conditions as the input for analyzing pixel heterogeneity using the semivariogram function. We strive to use satellite data from the same month as the ground observations whenever possible. In some cases, we resort to satellite data from months closely preceding or following the vegetation growing season to obtain clear-sky data to avoid cloud interference.

2.5. SRTM Data

The terrain significantly impacts the use of satellite observations to invert forest structure information. In this study, we utilized Shuttle Radar Topography Mission (SRTM) elevation data to calculate the slope, which served as an indicator of terrain ruggedness. The SRTM data is a valuable resource for understanding and analyzing the Earth's topography, which utilizes radar technology to detect the elevation of the land surface with exceptional accuracy [34]. It provides elevation information at an approximate spatial resolution of 30 m.

3. Methods

To improve the ability of MODIS multi-angular observations on forest AGB estimation, we aim to develop multi-angular indices based on typical-angular reflectances in red and NIR spectral bands. The workflow of this study is shown in Figure 2. We first used the semivariance function to conduct pixel homogeneity evaluation and selected the homogeneous pixels in our study area. Then, we set the BRDF models and SZAs to reconstruct the typical-angular reflectances of homogeneous MODIS pixels (e.g., hotspot, nadir, and darkspot) based on the MCD43A1 product. Using reconstructed typical-angular reflectances, we constructed multi-angular indices. Furthermore, we employed homogeneous MODIS pixels corresponding to field-measured biomass and forest cover density information, and we developed multi-angular indices to construct a forest AGB estimation equation. Finally, we evaluated the factors that influence the performance of our developed multi-angular indices, such as BRDF models, SZAs, terrain, and pixel forest cover density.

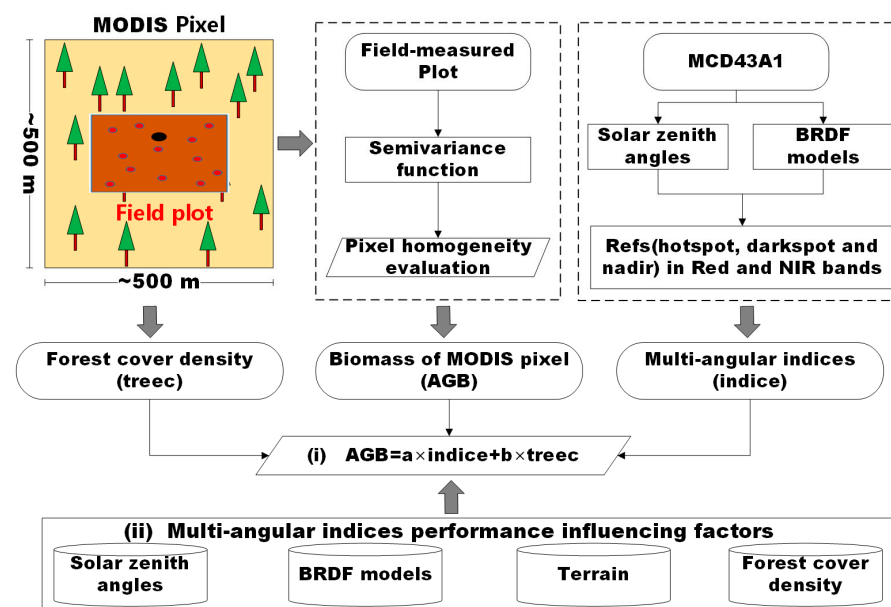


Figure 2. Workflow chart of this study method mainly includes two parts: (i) forest AGB estimation equation constructed based on multi-angular indices and (ii) evaluating factors that affected the performance of the multi-angular indices for forest AGB estimation.

The forest AGB estimation equation based on multi-angular indices is as follows:

$$AGB = a \cdot hotspot_indice + b \cdot nadir_indice + c \cdot darkspot_indice + d \cdot treec + e \quad (1)$$

where a , b , c , and d are weight coefficients for multi-angular indices; e is the constant term; $treec$ is the pixel forest cover information we defined; and $hotspot_indice$, $nadir_indice$, and $darkspot_indice$ refer to three multi-angular indices, they are the ratio indices of the hotspot, nadir, and darkspot reflectances in NIR and red spectral bands, respectively. For example, the $hotspot_indice$ was calculated by taking the hotspot reflectance in the NIR band as the numerator and the corresponding red band reflectance as the denominator.

3.1. Calculation of the Typical-Angular Reflectances

The BRDF model is expressed as a linear combination of isotropic, volumetric, and GO scattering kernels, with the general form as follows:

$$R(\theta, \vartheta, \varphi, \Lambda) = f_{iso}(\Lambda) + f_{vol}(\Lambda)K_{vol}(\theta, \vartheta, \varphi) + f_{geo}(\Lambda)K_{geo}(\theta, \vartheta, \varphi) \quad (2)$$

where f_{iso} , f_{vol} , and f_{geo} are the weight parameters that define the BRDF shape, reflecting the proportions of the three scattering components. K_{geo} and K_{vol} are the two functions constructed by view zenith (ϑ), illumination zenith (θ), and relative azimuth (φ); they describe the light scattering process within the canopy, that is, so-called the GO scattering kernel and volumetric scattering kernel.

Usually, there are various options for K_{geo} and K_{vol} , each designed to suit different observed situations. Therefore, the BRDF model that utilizes different combinations of kernels has a different spectral anisotropic reflectance. This situation indicates that the choice of K_{geo} and K_{vol} can have implications for its further application, such as the inversion of vegetation structure parameters.

To investigate the different configurations of the BRDF model and their effect on our method, we selected three different volume-scattering kernels and three GO kernels as the configurations for the BRDF models. The volume-scattering kernels we adopted were the RT kernel, RTN kernel, and RTC kernel; they are defined as follows:

$$K_{Rossthick} = \frac{(\frac{\pi}{2} - \zeta) \cos \zeta + \sin \zeta}{\cos \theta + \cos \vartheta} - \frac{\pi}{4} \tag{3}$$

$$K_{Rossthin} = \frac{(\frac{\pi}{2} - \zeta) \cos \zeta + \sin \zeta}{\cos \theta \cos \vartheta} - \frac{\pi}{2} \tag{4}$$

$$K_{RossthickChen} = \frac{(\frac{\pi}{2} - \zeta) \cos \zeta + \sin \zeta}{\cos \theta + \cos \vartheta} \times \left(1 + C_1 e^{-\frac{\zeta}{C_2}}\right) - \frac{\pi}{4} \tag{5}$$

$$\cos \zeta = \cos \theta \cos \vartheta + \sin \theta \sin \vartheta \cos \varphi \tag{6}$$

where ζ , defined in Equation (6), represents the phase angle, and C_1 and C_2 are two adjustable hotspot parameters; they are derived from POLDER observations [25]. The GO kernels we used were the LSR, LDR, and LTR kernels; they are defined as follows:

$$K_{LiSparseR} = o(\theta', \vartheta', \phi) - \sec \theta' - \sec \vartheta' + \frac{1}{2}(1 + \cos \zeta') \sec \vartheta' \sec \theta' \tag{7}$$

$$K_{LiDenseR} = \frac{(1 + \cos \zeta') \sec \vartheta' \sec \theta'}{\sec \theta' + \sec \vartheta' - o(\theta', \vartheta', \phi)} - 2 \tag{8}$$

$$K_{LiTransitR} = \begin{cases} K_{LiSparseR}, & B \leq 2 \\ \frac{2}{B} K_{LiSparseR}, & B > 2 \end{cases} \tag{9}$$

where o is the function describing the overlap between the shadows cast by the viewing and illumination geometries.

$$o(\theta', \vartheta', \phi) = \frac{1}{\pi}(t - \sin t \cdot \cos t)(\sec \theta' + \sec \vartheta') \tag{10}$$

In which the variables are defined as follows:

$$\cos t = \frac{h \sqrt{D^2 + (\tan \theta' \tan \vartheta' \sin \phi)^2}}{b \sec \theta' + \sec \vartheta'} \tag{11}$$

$$D = \left(\tan^2 \theta' + \tan^2 \vartheta' - 2 \tan \theta' \tan \vartheta' \cos \phi\right)^{1/2} \tag{12}$$

$$\cos \zeta' = \cos \theta' \cos \vartheta' + \sin \theta' \sin \vartheta' \cos \phi \tag{13}$$

$$\theta' = \tan^{-1}(b/r \tan \theta) \tag{14}$$

$$\vartheta' = \tan^{-1}(b/r \tan \vartheta) \tag{15}$$

where h/b and b/r are the relative height and shape of the described canopy, respectively. Furthermore, B in Equation (9) is defined as follows:

$$B = \sec \theta' + \sec \vartheta' - o(\theta', \vartheta', \phi) \tag{16}$$

Combining the volumetric scattering kernels and geometric-optical kernels mentioned earlier, we formulated a set of BRDF models (Table 1); these BRDF models were used to calculate MODIS typical-angular reflectances.

Table 1. BRDF models employed in this study.

K_{vol}	K_{geo}	LiSparseR	LiDenseR	LiTransitR
	RossThick	RTLSR	RTLDR	RTLTR
	RossThin	RTINLDR	RTINLSR	RTINLTR
	RossThickChen	RTCLSR		

3.2. Definition of Forest Cover Information of the MODIS Pixel

Forest coverage information, such as the forest cover proportion/density, is a key input for large-scale biomass mapping [35]. In other words, the accurate/calibrated forest coverage information may increase the possibility of producing fine biomass results. Here, we developed a strategy that combines pixel heterogeneity analysis and field-measured information to define the MODIS pixel forest coverage information. Firstly, we calculated the forest density of the sample plot based on the field survey data by dividing the forest tree numbers of the survey plot by the site area. Then, we assessed the homogeneity of each MODIS pixel using the semivariogram function. If the MODIS pixel was homogeneous, the forest density of the site scale was considered as a representative value for the actual forest coverage information of that MODIS pixel.

For the evaluation of the homogeneity of the MODIS pixel, we adopted the methodology from a prior study, using a clear-sky Landsat surface reflectance product that corresponds to each MODIS pixel as input for the semivariogram function. If the results indicated a sill value lower than 5.0×10^{-4} [32], we concluded that the land cover of the MODIS pixel was homogeneous. As an example (Figure 3), the sill value corresponding to the pixel with a 500 m spatial resolution is 0.95×10^{-4} , which is less than 5.0×10^{-4} . Therefore, the land cover of this MODIS pixel is homogeneous.

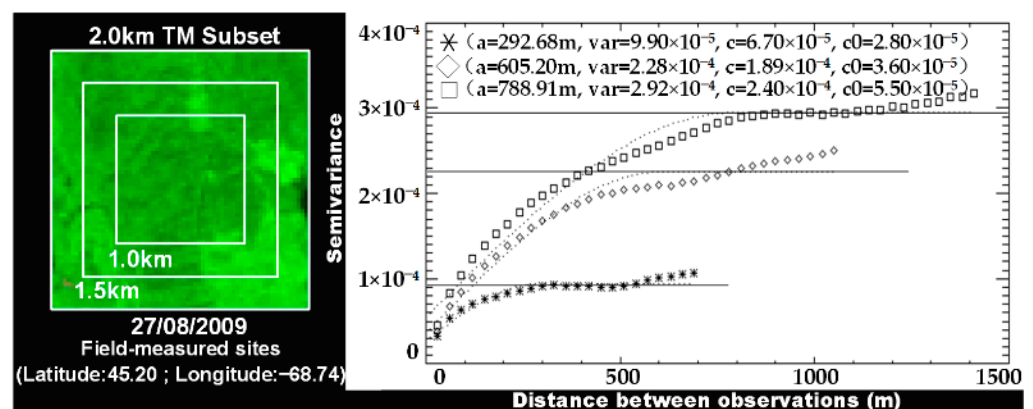


Figure 3. Evaluation of the homogeneity of the MODIS pixel using the semivariogram function based on the clear-sky Landsat surface reflectance product [19]. According to the variogram estimator, we take the MODIS pixel with a sill value (i.e., $c + c0$) of less than 5.0×10^{-4} as the homogeneous pixel.

3.3. Accuracy Validation

We employed the ordinary least squares regression (OLS) strategy to determine the coefficients of the biomass equation in Equation (1). Furthermore, we used the determination

coefficient (R^2) and root mean square error (RMSE) of these two indicators to validate the accuracy of our method:

$$R^2 = \frac{\sum_{i=1}^n (T_i - \bar{T})^2 - \sum_{i=1}^n (T_i - \bar{T}_i)^2}{\sum_{i=1}^n (T_i - \bar{T})^2} \quad (17)$$

$$RMSE = \sqrt{\frac{\sum_{i=1}^n (T_i - \bar{T}_i)^2}{n}} \quad (18)$$

where T_i is the estimated results, \bar{T}_i is the field-measured results, and n is the total data counts.

4. Results

4.1. Influence of Pixel Homogeneity and Terrain on Using MODIS Multi-Angular Indices for Forest AGB Estimation

We first examined the performance of our method on forest AGB estimation under an SZA equal to 45° (Figure 4). According to the results, we can note that no matter what kind of BRDF models were employed, the multi-angular indices cannot describe the variation of forest AGB well. The worst result explained only 29% of the variation in biomass, which, based on the RTCLSR BRDF model; results using other BRDF models can explain about 45% of the biomass variations, with RMSE around 66 Mg/ha. The following are some factors that may influence the ability of multi-angular indices to explain biomass variations, such as pixel heterogeneity and terrain factors. When we consider these two factors and filter out unsuitable sites (18 sites), the accuracy of using our constructed multi-angular indices to explain biomass was significantly improved. For example, using the RTCLSR BRDF model reconstructed typical-angular reflectances to construct multi-angular indices and then the estimated biomass, the accuracy increased from 29% to 72%, with an improved RMSE from 75 Mg/ha to 48 Mg/ha.

The pixel heterogeneity problem in using remote sensing data to estimate forest structure should be noted. In this study, we used field-measured biomass data from a 200×50 m plot as the ground truth for a 500 m MODIS pixel; there was a significant resolution disparity between these two datasets. As shown in Figure 5a, some field-measured plots corresponding to MODIS pixels display heterogeneity attributed to the presence of water bodies, bare land, and urban areas. In other words, these field-measured biomass data cannot represent the true situation of 500 m pixels well. Due to the above reason, we first filtered out sites that could not represent MODIS pixels according to the evaluation results from the semivariogram function. Additionally, there is extensive literature documenting the effect of rugged terrain on the BRDF anisotropic reflectances [36,37], which in turn should have a certain effect on its further application, such as forest structure estimation. We counted the slopes for each site; it could be noted that rugged terrain slopes had already happened (Figure 5b). To minimize the influence of rugged terrain on using BRDF data to estimate forest AGB in our study, we also filtered out sites with rugged slopes, such as those greater than 8 degrees.

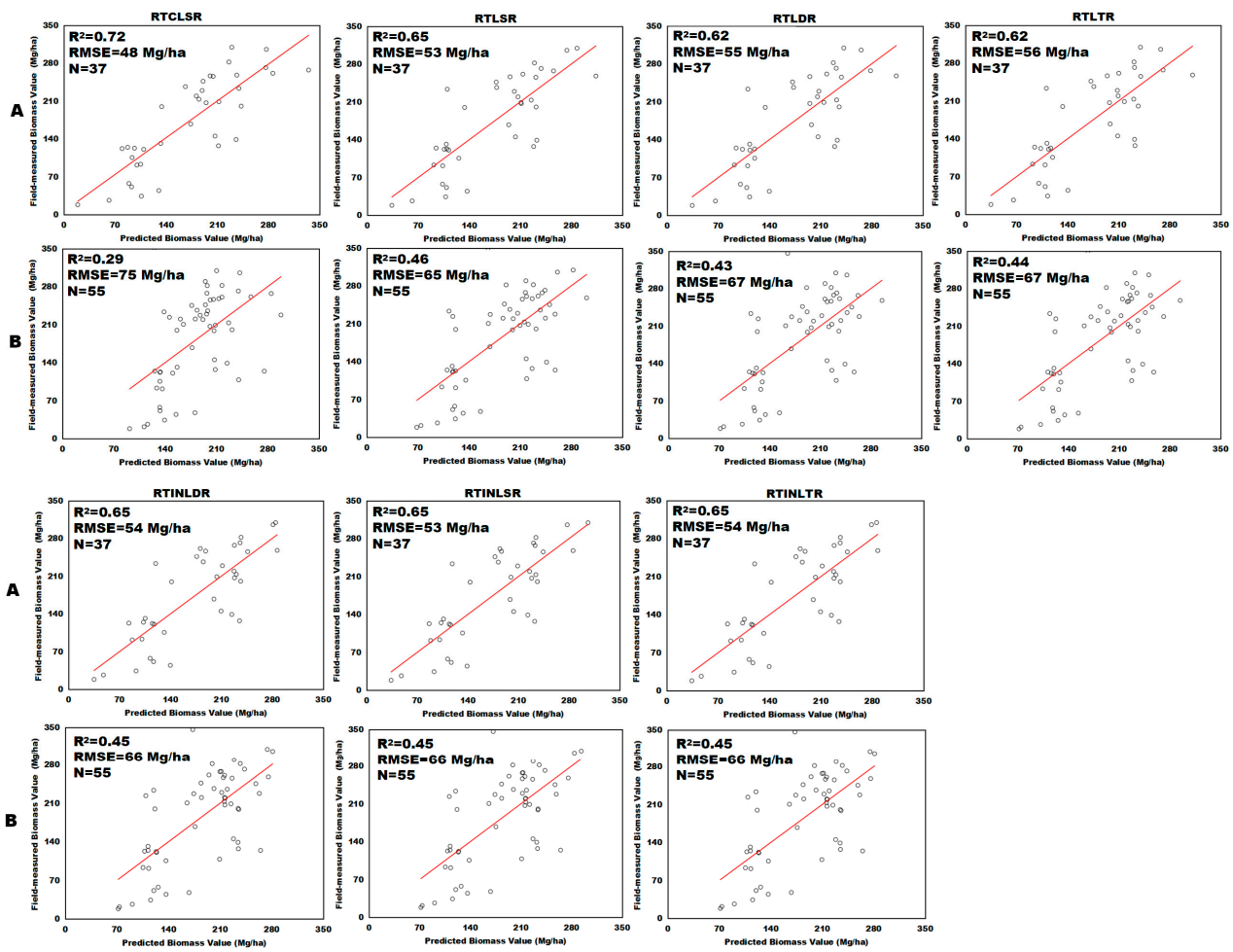
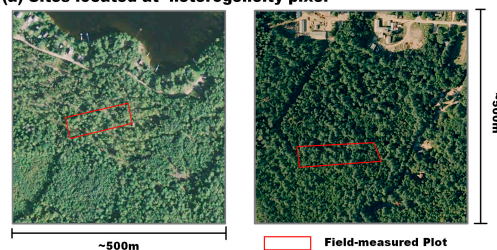


Figure 4. Performance of using multi-angular indices derived from different BRDF models under an SZ A equal to 45° combined with forest cover information to estimate forest AGB. Results showed in row (A) used the data located at homogeneous pixels with gentle terrain conditions; results showed in row (B) used all data located at study areas.

(a) Sites located at heterogeneity pixel



(b) Terrain information

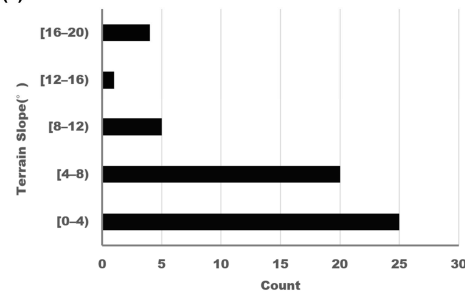


Figure 5. (a) The land cover situation of two MODIS pixels; the area outlined in red indicates the field-measured plots. (b) The counted slope information of all our study sites.

4.2. Influence of BRDF Models on Using MODIS Multi-Angular Indices for Forest AGB Estimation

We examined how the use of different BRDF models under an SZA of 45° affected the accuracy of our method for estimating forest AGB. The ground survey data used were located in homogeneous MODIS pixels with gentle terrain, involving a total of 37 sites (Appendix A). Most of the employed BRDF models did not show much difference in the accuracy of the biomass estimation; the difference was approximately an R^2 of 0.03 and a RMSE of 3 Mg/ha. The result based on a hot-revised BRDF model RTCLSR has a more eye-catching performance, with $R^2 = 0.72$ and $RMSE = 48$ Mg/ha. Furthermore, it can be noted that the weight parameters of the biomass prediction equations are quite different when employing different BRDF models, which happened in the condition when all these equations passed the F-test (Table 2). The above results indicate that the selection of different BRDF models potentially affects multi-angular indices' interpretation degree for biomass to a certain extent.

Table 2. The regression coefficients and Root Mean Square Error: $AGB = a \times hotspot_indices + b \times nadir_indice + c \times darkspot_indice + d \times treec + e$, where e is the intercept of the linear model.

BRDF Model	Regression Coefficients					F-Test	R^2	RMSE (Mg/ha)
	Hotspot Indice	Nadir Indice	Darkspot Indice	Tree Cover	Constant Term			
RTLSR	8.31	−6.74	7.14	0.12	−9.73	0	0.65	53
RTLDR	18.44	−52.40	43.18	0.12	−11.36	0	0.62	55
RTLTR	16.93	−44.66	37.17	0.12	−12.05	0	0.62	56
RTINLDR	−12.13	9.05	9.85	0.12	3.21	0	0.65	54
RTINLSR	−9.76	13.55	2.60	0.12	4.00	0	0.65	53
RTINLTR	−12.95	7.8	11.74	0.12	4.20	0	0.65	54
RTCLSR	12.24	4.65	4.56	0.12	−195.61	0	0.72	48

We draw the performance of different BRDF models for the reconstructed reflectances at the principal and cross-principal plane using a MODIS observation corresponding to a field-measured plot site (Figure 6). It can be noted that the reconstructed reflectance by using different BRDF models shows differences under the same SZA, such as typical-angular reflectances, which in turn influenced multi-angular indices. Therefore, the variation of the weight parameters is potentially caused by the differences in the factors and scenarios considered in the design of each kernel for BRDF models. For example, the GO kernel describes the shadow parts of the canopy, and this shadow information is also highly sensitive to variations of vegetation structure [38], such as the darkspot reflectance. We used the BRDF model involving the GO kernel LSR, which is designed for sparse canopies and ignores the shadow shading phenomenon between canopies. Therefore, the darkspot reflectance reconstructed from the BRDF model using the LSR kernel may show some difference in performance regarding weight parameters.

Furthermore, the forest coverage information plays a key role in our method (Figure 7a); the biomass inversion model can improve the accuracy by about 10% when considering the forest cover of the pixel. Additionally, the choice of different BRDF models has little effect on the importance of forest coverage information in our biomass inversion model. The above results also provide additional evidence for the importance of forest coverage information in retrieving biomass based on our multi-angular indices. The impact of field measurements on the validation accuracy of our method has already been noted. By analyzing the field-measured data and incorporating the validation results (Figure 7b), we found that some outliers in the validation results are located at the sites where there are a large number of dead trees. For example, approximately 900 trees were counted in site 4, with 179 dead trees in this site. In this study, nearly all sites included dead trees, and we did not exclude them when estimating the field biomass data. There is a large gap in the spectral characteristics between living trees and dead trees, and our method relies on the

spectral information of forests to estimate biomass. Therefore, we can reasonably consider that these dead trees have a certain effect on the validation of our method. In other words, the reliability of our method may be higher than our validation results.

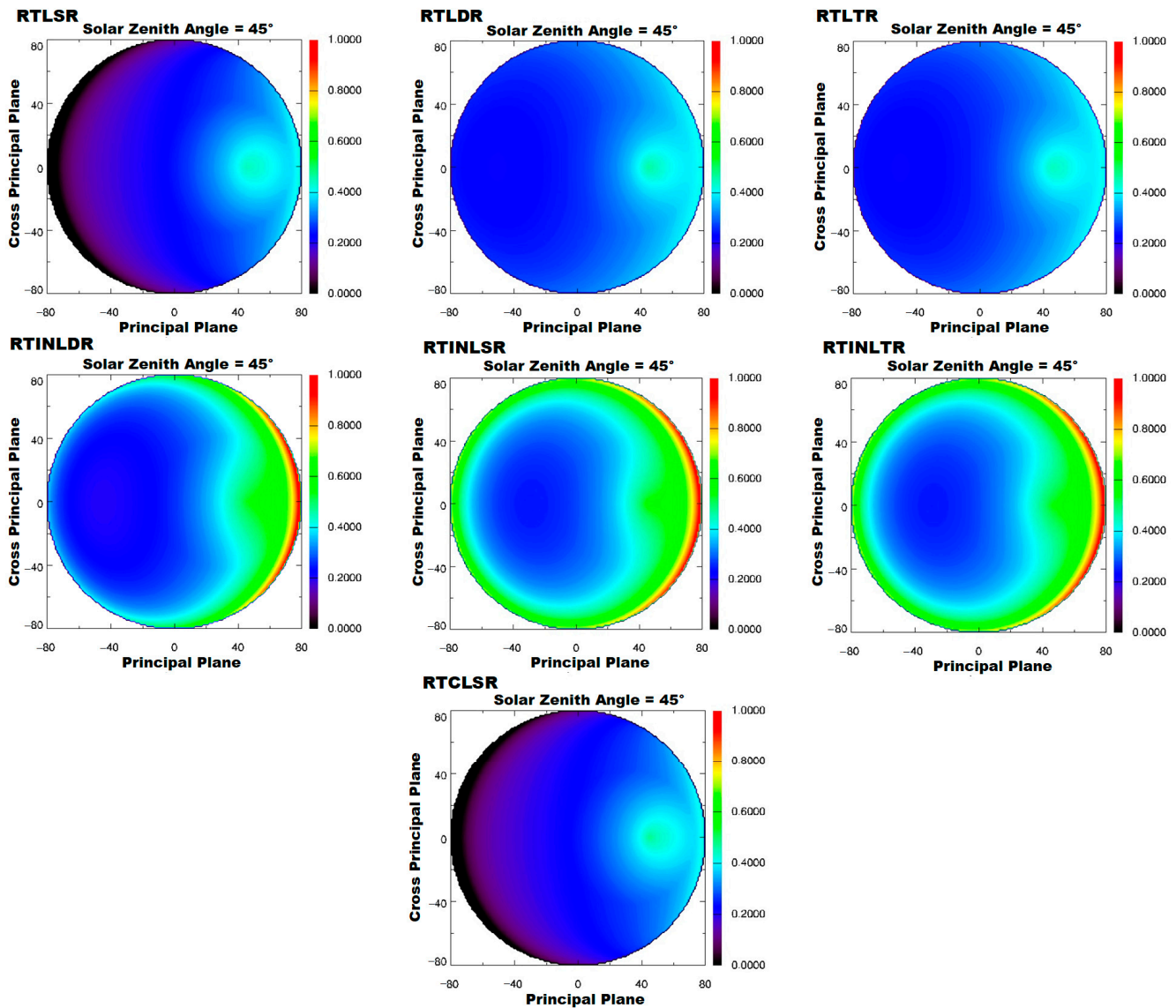


Figure 6. The performance of reconstructed MODIS observed reflectances at the principal and cross-principal plane by using RTLSR, RTLDR, RTLTR, RTINLDR, RTINLSR, RTINLTR, and RTCLSR. These seven different BRDF models were used under an SZA of 45°.

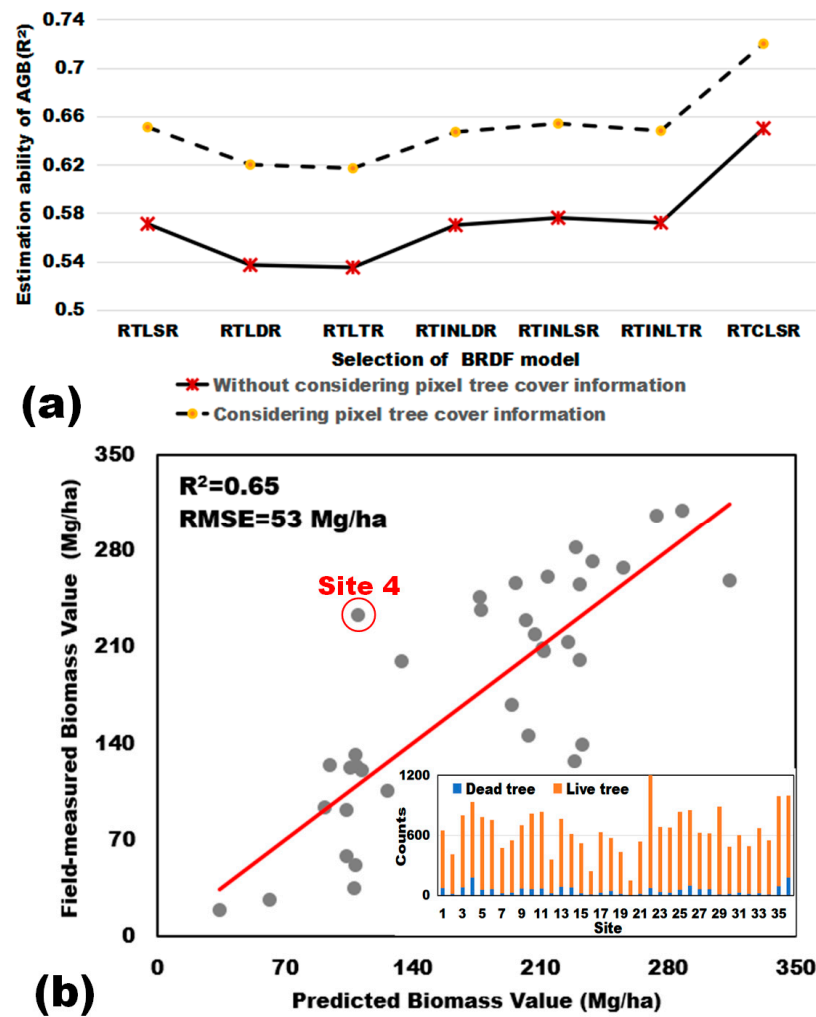


Figure 7. (a) The assessment results of the impact of choosing different BRDF models on the inversion of forest AGB by our method; (b) the linear regression results for estimating forest AGB based on the RTLSR model. Some obvious outliers may be caused by the dead trees counted in the field-observed sites, such as site 4.

4.3. Influence of Solar Zenith Angle on Using MODIS Multi-Angular Indices for Forest AGB Estimation

As shown in Figure 8, the BRDF shape shows differences under different SZAs; the reconstructed MODIS reflectances contain differences when the SZA is different, such as hotspot, nadir, and darkspot reflectances. The above differences will cause variations in the multi-angular indices and then affect the biomass estimation. Taking the RTCLSR BRDF model as an example, it can be seen that there will be a relatively obvious hotspot effect when the observation is conducted at a relatively mid-angle, such as 45° . Hotspot reflectance plays an important role in explaining forest structure information, such as canopy height and clumping index, and has been reported in many studies. Our results further prove the importance of hotspot observations; the coefficient of *hotspot_index* has a significant weight in the biomass estimation equation (Table 2). However, the hotspot effect does not perform strongly at a larger viewing angle, such as 60° , which in turn should be limited in forest structure inversion. Furthermore, it can be noted that although the hotspot effect is obvious at low observation angles, such as when the SZA equals 30° , the ranges of BRFs in the hemispheric space are small. The small range of BRFs will have a small range of multi-angular indices, which may be limitations in the ability to interpret ranges in forest structure information, such as biomass.

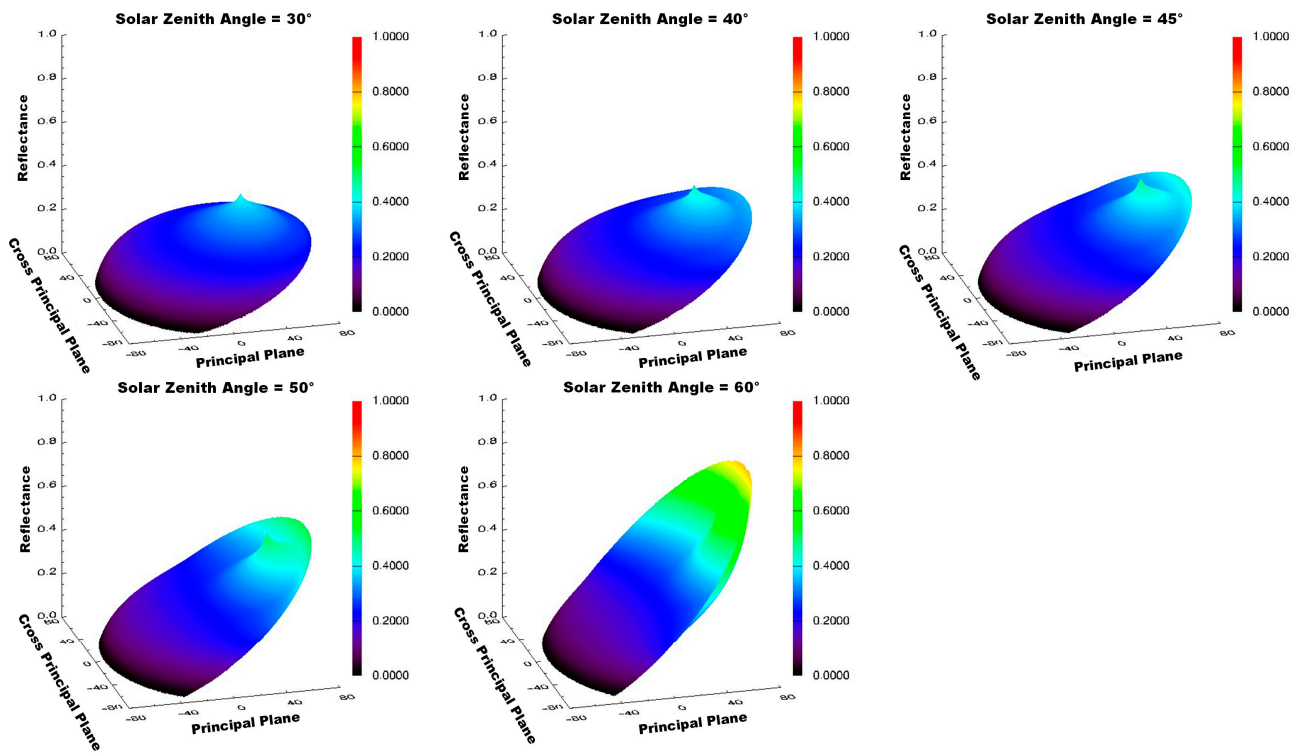


Figure 8. The MODIS observed 3D BRDF shapes reconstructed based on the RTCLSR BRDF model under SZA at 30°, 40°, 45°, 50°, and 60°.

Here, we examined the SZA effects on using MODIS multi-angular indices to estimate forest AGB. Figure 9 compares the validation results of using multi-angular indices that were constructed based on different BRDF models and SZA values. Among all the results, our method has the best performance based on the RTCLSR BRDF model under an SZA of around 45° ($R^2 \approx 0.72$, RMSE ≈ 48 Mg/ha). In terms of the remaining BRDF models, it can be noted that constructed multi-angular indices at SZA = 45° showed a relatively better performance for biomass estimation compared to results under other SZAs. There are two reasons for the above results: (i) The performance of the BRDF model is unstable at large SZAs. For example, the LSR kernel is intended to describe sparse canopies and shadow conditions, which can lead to its physical mechanism being less suitable for larger SZAs. When a model loses its physical meaning, it generates unreasonable modeling results, which subsequently hinders its practical application. (ii) At small SZAs, the multi-angle reflectances, such as darkspot reflectance, exhibit a relatively weak shadow effect. However, the shadow information contains certain vegetation structure information. Therefore, losing part of the shadow information may affect the accuracy of biomass inversion based on multi-angular indices.

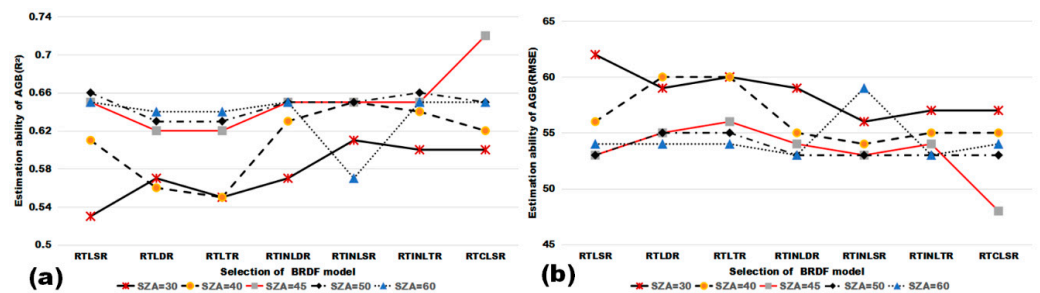


Figure 9. Influence of SZA on the accuracy of using MODIS multi-angular indices on forest AGB estimation. (a) The evaluation results with determined coefficients. (b) The evaluation results with root mean square error.

5. Discussion

We have examined the capability of using MODIS multi-angular indices we developed to explain the variation of forest AGB; we also discussed the influence of using different BRDF models and SZAs. Although our experimental results can be used as evidence to choose a suitable BRDF model and SZA to construct MODIS multi-angular indices to estimate forest AGB, some uncertainties or limitations can be improved in further studies.

In terms of the BRDF model selection, ideally, we should choose volumetric scattering kernels and GO kernels for the BRDF model according to the observed scenario. This is because it can make the physical conditions on which the kernels in the BRDF model are based fully valid, allowing for a more accurate reconstruction of reflectance information. For example, the GO kernel LiSparse is suitable for sparse canopy structures [8,23,24], while LiDense is suitable for dense canopy structures [23]. Some research has also found some limitations on the use of BRDF models, such as the fact that the RT kernel does not perform optimally on the hotspot [26]. This is because the RT kernel is derived from a horizontally homogeneous canopy and does not consider the relationship between the incident and observation geometry. The RTCLSR BRDF model improves hotspot accuracy by improving the volume scattering kernel Rossthick by adding a hotspot factor function [26]. Hotspot reflectance has been proven to be closely related to vegetation structure [12,21,39]. Our results also prove the above conclusion that using constructed multi-angular indices based on the RTCLSR model has the best performance in estimating forest biomass among the BRDF models we used. Although we have explored the influence of BRDF models on the inversion of forest biomass based on the MODIS data, the limited available ground observations restrict exploration of the differences in BRDF model selection for different canopy conditions regarding biomass inversion.

The SZA varies at different latitudes, which results in differences in the observation directions of hotspot or darkspot at different latitudes. In other words, due to variations in the SZA, the constructed multi-angular indices will be varied. Therefore, the significant differences in the SZA are likely to propagate the use of multi-angular indices for further applications, such as the inversion of forest AGB information. Considering the reasons mentioned above, we believe it is necessary to discuss and determine the most suitable solar incidence angles for estimating forest structure parameters when using multi-angular indices under different latitudes. However, as there was a lack of field-measured data in this study, we did not explore this aspect.

We utilized field-measured data as the ground truth for MODIS pixels, such as tree cover and forest biomass information. However, there is a gap in resolution between the field-measured plot and the MODIS pixel (50 m × 200 m vs. 500 m × 500 m). Field-measured plots provide valuable ground-level data, but their ability to accurately represent an entire pixel varies. The accuracy depends on factors such as plot size, placement, and the spatial heterogeneity of the area being studied [40,41]. While field plots can provide detailed information about specific locations, their ability to represent an entire pixel's characteristics may be limited. Therefore, there are uncertainties in using smaller-scale ground observations to represent coarser resolution MODIS pixels [42–44]. In order to minimize the above uncertainties, we employed the semivariance function using Landsat surface reflectance data to evaluate the homogeneity of MODIS pixels; only homogeneous MODIS pixels were employed for experiment analysis. Although this strategy can greatly improve the reliability of ground observations representing the true state of pixels [21,45], it is obvious that relying solely on the spectral information from Landsat images proves inadequate in accurately distinguishing certain elements on the Earth's surface. For instance, the spectral properties of grass and canopy are strikingly similar, resulting in significant uncertainty when estimating biomass in our research. High-resolution airborne lidar equipment provides the opportunity for obtaining the accurate 3D structure of the forest canopy, which should be a good option to replace ground-based observations in future studies. Nearly continuous observation can avoid the problem of pixel representativeness to a

certain extent as the true value for larger-scale pixels, thereby improving experimental accuracy.

Overall, this study has proved the feasibility of using MODIS multi-angular indices we developed for the inversion of forest biomass and has provided insights into the impact of BRDF model selection and SZA settings on forest AGB inversion. However, there are limitations in the experiments due to the constraints of ground observation data, such as mentioned above. They should further improve when sufficient field-measured or airborne-observed data are available. The supplementation can further solidify the theoretical basis for the production of large-scale forest biomass products using MODIS BRDF data.

6. Conclusions

In this study, we explored the effectiveness of using MODIS multi-angular observations for forest AGB estimation. The developed multi-angular indices based on typical-angular reflectances in red and NIR bands demonstrate the capacity to explain the variation of forest AGB. Incorporating the pixel forest cover information in the biomass estimation equation can increase the prediction accuracy by about 10%. Furthermore, we evaluated the impact of using different BRDF configurations, such as the selection of kernels and SZA values, on the accuracy of our method. The results indicate that the selection of different kernels for the BRDF model influences the weight parameters of the biomass inversion equation; however, it has little effect on the estimated biomass. An optimal stability and performance for our method can be achieved by setting the SZA to around 45°. Overall, the integration of developed multi-angular indices and accurate pixel forest cover information is reliable for forest AGB estimation. Such an approach holds promise as a valuable choice for producing global forest AGB products.

Author Contributions: Conceptualization, L.C. and R.X.; data curation, J.Z., Y.D. (Yiqun Dai) and L.C.; formal analysis, J.Z. and L.C.; funding acquisition, L.C.; software, J.Z., M.S. and Y.D. (Yiqun Dai); writing—original draft, L.C.; and writing—review & editing, L.C., Z.Z., L.H., H.Z., Y.D. (Yadong Dong), X.Z. and K.Z. All authors have read and agreed to the published version of the manuscript.

Funding: This work was supported by the Tianjin Science and Technology Plan Project under Grant 22JCQNJC01420 and the Chunhui Project Foundation of the Education Department of China under Grant 202200324.

Data Availability Statement: All satellite remote sensing data used in this study are openly and freely available. The MODIS BRDF product (MCD43A1) is available at <https://search.earthdata.nasa.gov/search> (accessed on 1 October 2023). The SRTM data is available at <http://srtm.csi.cgiar.org/srtmdata/> (accessed on 1 October 2023). The clear sky Landsat surface reflectance data are available at <https://earthexplorer.usgs.gov/> (accessed on 1 October 2023). The field-based forest biomass data are available at https://daac.ornl.gov/cgi-bin/dsvviewer.pl?ds_id=1046 (accessed on 1 October 2023).

Acknowledgments: The field-measured biomass data was supported by the North American Carbon Program (NACP). We thank the NACP for its open policy that allowed our experiments to proceed smoothly.

Conflicts of Interest: The authors declare no conflicts of interest.

Appendix A

Table A1. The detailed information of field-measured sites, including location information, measured biomass, measured time, and the composition of measured biomass.

Forest	Location		Time	Composition of Biomass		Biomass (Mg ha ⁻¹)
	Latitude (°)	Longitude (°)		Dead Tree Counts	Live Tree Counts	
Barttle	44.053185	−71.310543	11 July 2009	75	648	200.59
Barttle	44.054021	−71.300303	13 July 2009	17	648	229.44
Barttle	44.054162	−71.289812	12 July 2009	82	800	255.46
Harvard	42.534074	−72.182013	25 June 2009	179	936	305.44
Harvard	42.536547	−72.175841	24 July 2009	55	785	139.03
Harvard	42.538096	−72.177597	27 July 2009	63	753	208.88
Harvard	42.536557	−72.172724	23 July 2009	24	475	256.43
Harvard	42.536516	−72.179817	14 July 2009	27	551	271.89
Harvard	42.540983	−72.170486	28 July 2009	66	702	219.34
Harvard	42.540467	−72.183034	16 July 2009	61	817	127.38
Harvard	42.539223	−72.187066	17 July 2009	70	834	282.08
Harvard	42.551416	−72.176897	26 July 2009	22	359	145.36
Harvard	42.480697	−72.174601	25 July 2009	83	763	206.87
Harvard	42.508234	−72.250973	27 July 2009	77	612	309.28
Harvard	42.512857	−72.205741	25 July 2009	20	520	236.60
Howland	45.22755	−68.725911	20 August 2009	12	242	26.83
Howland	45.225188	−68.724381	24 August 2009	26	629	34.39
Howland	45.222658	−68.716496	25 August 2009	42	571	91.87
Howland	45.214881	−68.735791	24 August 2009	18	432	57.80
Howland	45.214646	−68.709366	26 August 2009	0	148	18.65
Howland	45.210844	−68.737554	19 August 2009	14	541	105.80
Howland	45.203327	−68.741371	19 August 2009	76	1212	167.57
Howland	45.152076	−68.735178	27 August 2009	35	687	131.73
Howland	45.147732	−68.718229	27 August 2009	30	677	122.98
Hubbard Brook	43.936143	−71.741518	22 July 2009	52	614	267.26
Hubbard Brook	43.940344	−71.778636	20 July 2009	57	833	261.25
Hubbard Brook	43.945148	−71.709622	27 July 2009	97	850	257.82
Hubbard Brook	43.941246	−71.703841	18 July 2009	63	628	246.54
Hubbard Brook	43.947527	−71.704189	24 July 2009	60	618	213.38
Penobscot	44.871236	−68.626076	25 August 2009	97	687	233.43
Penobscot	44.858001	−68.620421	24 August 2009	12	886	44.76
Penobscot	44.851611	−68.618074	18 August 2009	17	484	124.65
Penobscot	44.850592	−68.613788	19 August 2009	29	604	51.60
Penobscot	44.848417	−68.615501	19 August 2009	13	491	122.27
Penobscot	44.84406	−68.619475	20 August 2009	19	672	120.84
Penobscot	44.844779	−68.614519	20 August 2009	10	549	93.37
Penobscot	44.835663	−68.599269	26 August 2009	94	994	199.65

References

- Duncanson, L.; Armston, J.; Disney, M.; Avitabile, V.; Barbier, N.; Calders, K.; Carter, S.; Chave, J.; Herold, M.; Crowther, T.W. The Importance of Consistent Global Forest Aboveground Biomass Product Validation. *Surv. Geophys.* **2019**, *40*, 979–999. [\[CrossRef\]](#)
- García, M.; Riaño, D.; Chuvieco, E.; Danson, F.M. Estimating Biomass Carbon Stocks for a Mediterranean Forest in Central Spain Using LiDAR Height and Intensity Data. *Remote Sens. Environ.* **2010**, *114*, 816–830. [\[CrossRef\]](#)
- Chen, Y.; Feng, X.; Fu, B.; Ma, H.; Zohner, C.M.; Crowther, T.W.; Huang, Y.; Wu, X.; Wei, F. Maps with 1 km Resolution Reveal Increases in above-and Belowground Forest Biomass Carbon Pools in China over the Past 20 Years. *Earth Syst. Sci. Data* **2023**, *15*, 897–910. [\[CrossRef\]](#)
- Li, L.; Zhou, B.; Liu, Y.; Wu, Y.; Tang, J.; Xu, W.; Wang, L.; Ou, G. Reduction in Uncertainty in Forest Aboveground Biomass Estimation Using Sentinel-2 Images: A Case Study of *Pinus densata* Forests in Shangri-La City, China. *Remote Sens.* **2023**, *15*, 559. [\[CrossRef\]](#)
- Moghimi, A.; Darestani, A.T.; Mostofi, N.; Fathi, M.; Amani, M. Improving Forest Above-Ground Biomass Estimation Using Genetic-Based Feature Selection from Sentinel-1 and Sentinel-2 Data (Case Study of the Noor Forest Area in Iran). *Kuwait J. Sci.* **2023**, 100159. [\[CrossRef\]](#)

6. Chen, J.M.; Leblanc, S.G. A Four-Scale Bidirectional Reflectance Model Based on Canopy Architecture. *IEEE Trans. Geosci. Remote* **1997**, *35*, 1316–1337. [[CrossRef](#)]
7. Gerard, F.F.; North, P. Analyzing the Effect of Structural Variability and Canopy Gaps on Forest BRDF Using a Geometric-Optical Model. *Remote Sens. Environ.* **1997**, *62*, 46–62. [[CrossRef](#)]
8. Li, X.; Strahler, A.H. Geometric-Optical Bidirectional Reflectance Modeling of the Discrete Crown Vegetation Canopy: Effect of Crown Shape and Mutual Shadowing. *IEEE Trans. Geosci. Remote* **1992**, *30*, 276–292. [[CrossRef](#)]
9. Asner, G.P. Contributions of Multi-View Angle Remote Sensing to Land-Surface and Biogeochemical Research. *Remote Sens. Rev.* **2000**, *18*, 137–162. [[CrossRef](#)]
10. Liu, X.; Liu, L. Influence of the Canopy Brdf Characteristics and Illumination Conditions on the Retrieval of Solar-induced Chlorophyll Fluorescence. *Int. J. Remote Sens.* **2018**, *39*, 1782–1799. [[CrossRef](#)]
11. Wang, Q.; Pang, Y.; Li, Z.; Chen, E.; Sun, G.; Tan, B. Improvement and Application of the Conifer Forest Multiangular Hybrid GORT Model MGeoSAIL. *IEEE Trans. Geosci. Remote* **2013**, *51*, 5047–5059. [[CrossRef](#)]
12. Cui, L.; Jiao, Z.; Dong, Y.; Sun, M.; Zhang, X.; Yin, S.; Ding, A.; Chang, Y.; Guo, J.; Xie, R. Estimating Forest Canopy Height Using MODIS BRDF Data Emphasizing Typical-Angle Reflectances. *Remote Sens.* **2019**, *11*, 2239. [[CrossRef](#)]
13. Muukkonen, P.; Heiskanen, J. Biomass Estimation over a Large Area Based on Standwise Forest Inventory Data and ASTER and MODIS Satellite Data: A Possibility to Verify Carbon Inventories. *Remote Sens. Environ.* **2007**, *107*, 617–624. [[CrossRef](#)]
14. Chopping, M.; Moisen, G.G.; Su, L.; Laliberte, A.; Rango, A.; Martonchik, J.V.; Peters, D.P. Large Area Mapping of Southwestern Forest Crown Cover, Canopy Height, and Biomass Using the NASA Multiangle Imaging Spectro-Radiometer. *Remote Sens. Environ.* **2008**, *112*, 2051–2063. [[CrossRef](#)]
15. Chopping, M.; Schaaf, C.B.; Zhao, F.; Wang, Z.; Nolin, A.W.; Moisen, G.G.; Martonchik, J.V.; Bull, M. Forest Structure and Aboveground Biomass in the Southwestern United States from MODIS and MISR. *Remote Sens. Environ.* **2011**, *115*, 2943–2953. [[CrossRef](#)]
16. Chopping, M.; Wang, Z.; Schaaf, C.; Bull, M.A.; Duchesne, R.R. Forest Aboveground Biomass in the Southwestern United States from a MISR Multi-Angle Index, 2000–2015. *Remote Sens Environ* **2022**, *275*, 112964. [[CrossRef](#)]
17. Sharma, R.C. Vegetation Structure Index (VSI): Retrieving Vegetation Structural Information from Multi-Angular Satellite Remote Sensing. *J. Imaging* **2021**, *7*, 84. [[CrossRef](#)]
18. Wang, Q.; Pang, Y.; Li, Z.; Sun, G.; Chen, E.; Ni-Meister, W. The Potential of Forest Biomass Inversion Based on Vegetation Indices Using Multi-Angle CHRIS/PROBA Data. *Remote Sens.* **2016**, *8*, 891. [[CrossRef](#)]
19. Cui, L.; Sun, M.; Jiao, Z.; Park, J.; Agca, M.; Zhang, H.; He, L.; Dai, Y.; Dong, Y.; Zhang, X. Effectiveness of the Reconstructed MODIS Typical-Angle Reflectances on Forest Biomass Estimation. *Remote Sens.* **2022**, *14*, 5475. [[CrossRef](#)]
20. Chang, Y.; Jiao, Z.; Zhang, X.; Mei, L.; Dong, Y.; Yin, S.; Cui, L.; Ding, A.; Guo, J.; Xie, R. Assessment of Improved Ross–Li BRDF Models Emphasizing Albedo Estimates at Large Solar Angles Using POLDER Data. *IEEE Trans. Geosci. Remote* **2020**, *59*, 9968–9986. [[CrossRef](#)]
21. Wei, S.; Fang, H.; Schaaf, C.B.; He, L.; Chen, J.M. Global 500 m Clumping Index Product Derived from MODIS BRDF Data (2001–2017). *Remote Sens. Environ.* **2019**, *232*, 111296. [[CrossRef](#)]
22. Roujean, J.L.; Leroy, M.; Deschamps, P.Y. A Bidirectional Reflectance Model of the Earth’s Surface for the Correction of Remote Sensing Data. *J. Geophys. Res. Atmos.* **1992**, *97*, 20455–20468. [[CrossRef](#)]
23. Wanner, W.; Li, X.; Strahler, A.H. On the Derivation of Kernels for Kernel-Driven Models of Bidirectional Reflectance. *J. Geophys. Res. Atmos.* **1995**, *100*, 21077–21089. [[CrossRef](#)]
24. Lucht, W.; Schaaf, C.B.; Strahler, A.H. An Algorithm for the Retrieval of Albedo from Space Using Semiempirical BRDF Models. *IEEE Trans. Geosci. Remote* **2000**, *38*, 977–998. [[CrossRef](#)]
25. Li, X.; Gao, F.; Chen, L.; Strahler, A.H. Derivation and Validation of a New Kernel for Kernel-Driven BRDF Models. In *Remote Sensing for Earth Science, Ocean, and Sea Ice Application*; SPIE: Bellingham, WA, USA, 1999; Volume 3868, pp. 368–379.
26. Jiao, Z.; Schaaf, C.B.; Dong, Y.; Román, M.; Hill, M.J.; Chen, J.M.; Wang, Z.; Zhang, H.; Saenz, E.; Poudyal, R. A Method for Improving Hotspot Directional Signatures in BRDF Models Used for MODIS. *Remote Sens. Environ.* **2016**, *186*, 135–151. [[CrossRef](#)]
27. Cook, B.; Dubayah, R.O.; Hall, F.G.; Nelson, R.F.; Ranson, K.J.; Strahler, A.H.; Siqueira, P.; Simard, M.; Griffith, P. *NACP New England and Sierra National Forests Biophysical Measurements: 2008–2010*; ORNL DAAC: Oak Ridge, TN, USA, 2011. [[CrossRef](#)]
28. Young, H.E.; Ribe, J.H.; Wainwright, K. *Weight Tables for Tree and Shrub Species in Maine*; Life Sciences and Agriculture Experiment Station, University of Maine at Orono: Orono, ME, USA, 1980; p. 84.
29. MCD43A1 v061 MODIS/Terra+Aqua BRDF/Albedo Model Parameters Daily L3 Global 500 m SIN Grid. Available online: <https://lpdaac.usgs.gov/products/mcd43a1v061/> (accessed on 1 October 2023).
30. Masek, J.G.; Vermote, E.F.; Saleous, N.E.; Wolfe, R.; Hall, F.G.; Huemmrich, K.F.; Gao, F.; Kutler, J.; Lim, T. A Landsat Surface Reflectance Dataset for North America, 1990–2000. *IEEE Geosci. Remote Sens. Lett.* **2006**, *3*, 68–72. [[CrossRef](#)]
31. Vermote, E.; Justice, C.; Claverie, M.; Franch, B. Preliminary Analysis of the Performance of the Landsat 8/OLI Land Surface Reflectance Product. *Remote Sens. Environ.* **2016**, *185*, 46–56. [[CrossRef](#)]
32. Wang, Z.; Schaaf, C.B.; Strahler, A.H.; Chopping, M.J.; Román, M.O.; Shuai, Y.; Woodcock, C.E.; Hollinger, D.Y.; Fitzjarrald, D.R. Evaluation of MODIS Albedo Product (MCD43A) over Grassland, Agriculture and Forest Surface Types during Dormant and Snow-Covered Periods. *Remote Sens. Environ.* **2014**, *140*, 60–77. [[CrossRef](#)]

33. Zawadzki, J.; Cieszewski, C.J.; Zasada, M. Semivariogram Analysis of Landsat 5 TM Textural Data for Loblolly Pine Forests. *J. For. Sci.* **2005**, *51*, 47–59. [[CrossRef](#)]
34. Farr, T.G.; Rosen, P.A.; Caro, E.; Crippen, R.; Duren, R.; Hensley, S.; Kobrick, M.; Paller, M.; Rodriguez, E.; Roth, L.; et al. The Shuttle Radar Topography Mission. *Rev. Geophys.* **2007**, *45*, 2005RG000183. [[CrossRef](#)]
35. Du, L.; Zhou, T.; Zou, Z.; Zhao, X.; Huang, K.; Wu, H. Mapping Forest Biomass Using Remote Sensing and National Forest Inventory in China. *Forests* **2014**, *5*, 1267–1283. [[CrossRef](#)]
36. Wen, J.; You, D.; Han, Y.; Lin, X.; Wu, S.; Tang, Y.; Xiao, Q.; Liu, Q. Estimating Surface BRDF/Albedo over Rugged Terrain Using an Extended Multisensor Combined BRDF Inversion (EMCBI) Model. *IEEE Geosci. Remote Sens. Lett.* **2022**, *19*, 2503505. [[CrossRef](#)]
37. Wen, J.; Liu, Q.; Xiao, Q.; Liu, Q.; You, D.; Hao, D.; Wu, S.; Lin, X. Characterizing Land Surface Anisotropic Reflectance Over Rugged Terrain: A Review of Concepts and Recent Developments. *Remote Sens.* **2018**, *10*, 370. [[CrossRef](#)]
38. Pellikka, P.; King, D.J.; Leblanc, S.G. Quantification and Reduction of Bidirectional Effects in Aerial CIR Imagery of Deciduous Forest Using Two Reference Land Surface Types. *Remote Sens. Rev.* **2000**, *19*, 259–291. [[CrossRef](#)]
39. Fang, H. Canopy Clumping Index (CI): A Review of Methods, Characteristics, and Applications. *Agric. Forest Meteorol.* **2021**, *303*, 108374. [[CrossRef](#)]
40. Wang, L.; Yang, R.; Tian, Q.; Yang, Y.; Zhou, Y.; Sun, Y.; Mi, X. Comparative Analysis of GF-1 WFV, ZY-3 MUX, and HJ-1 CCD Sensor Data for Grassland Monitoring Applications. *Remote Sens.* **2015**, *7*, 2089–2108. [[CrossRef](#)]
41. Li, J.; Pei, Y.; Zhao, S.; Xiao, R.; Sang, X.; Zhang, C. A Review of Remote Sensing for Environmental Monitoring in China. *Remote Sens.* **2020**, *12*, 1130. [[CrossRef](#)]
42. Wang, S.; Li, X.; Ge, Y.; Jin, R.; Ma, M.; Liu, Q.; Wen, J.; Liu, S. Validation of Regional-Scale Remote Sensing Products in China: From Site to Network. *Remote Sens.* **2016**, *8*, 980. [[CrossRef](#)]
43. Coll, C.; Caselles, V.; Galve, J.M.; Valor, E.; Niclos, R.; Sánchez, J.M.; Rivas, R. Ground Measurements for the Validation of Land Surface Temperatures Derived from AATSR and MODIS Data. *Remote Sens. Environ.* **2005**, *97*, 288–300. [[CrossRef](#)]
44. Fang, H.; Baret, F.; Plummer, S.; Schaepman Strub, G. An Overview of Global Leaf Area Index (LAI): Methods, Products, Validation, and Applications. *Rev. Geophys.* **2019**, *57*, 739–799. [[CrossRef](#)]
45. Lévesque, J.; King, D.J. Airborne Digital Camera Image Semivariance for Evaluation of Forest Structural Damage at an Acid Mine Site. *Remote Sens. Environ.* **1999**, *68*, 112–124. [[CrossRef](#)]

Disclaimer/Publisher’s Note: The statements, opinions and data contained in all publications are solely those of the individual author(s) and contributor(s) and not of MDPI and/or the editor(s). MDPI and/or the editor(s) disclaim responsibility for any injury to people or property resulting from any ideas, methods, instructions or products referred to in the content.